Photoassociation of Long-Range *nD* Rydberg Molecules

D. A. Anderson,* S. A. Miller, and G. Raithel
Department of Physics, University of Michigan, Ann Arbor, Michigan 48109, USA
(Received 6 January 2014; published 23 April 2014)

We observe long-range homonuclear diatomic nD Rydberg molecules photoassociated out of an ultracold gas of ^{87}Rb atoms for $34 \leq n \leq 40$. The measured ground-state binding energies of $^{87}\mathrm{Rb}(nD + 5S_{1/2})$ molecular states are larger than those of their $^{87}\mathrm{Rb}(nS + 5S_{1/2})$ counterparts, which shows the dependence of the molecular bond on the angular momentum of the Rydberg atom. We exhibit the transition of $^{87}\mathrm{Rb}(nD + 5S_{1/2})$ molecules from a molecular-binding-dominant regime at low n to a fine-structure-dominant regime at high n [akin to Hund's cases (a) and (c), respectively]. In the analysis, the fine structure of the nD Rydberg atom and the hyperfine structure of the $5S_{1/2}$ atom are included.

DOI: 10.1103/PhysRevLett.112.163201 PACS numbers: 34.50.Cx, 31.10.+z, 33.80.Rv, 34.20.Cf

Cold atomic systems have opened new frontiers at the interface of atomic and molecular physics. Of particular interest are a recently discovered class of long-range, homonuclear Rydberg molecules [1,2]. Formed via an attractive interaction between a Rydberg electron and a ground-state atom [1], these molecules are among the largest ever observed with internuclear separations of several thousand Bohr radii. Their distinctive binding mechanism, which is unlike conventional covalent, ionic, and van der Waals bonds between ground-state atoms, results in loosely bound molecules whose properties mimic those of their constituent Rydberg atoms. The discovery of these molecular bonds has been likened to a new ultracold chemistry [3] and has spurred a significant amount of theoretical [4,5] and experimental interest [6–9]. Nondegenerate, low angular momentum Rydberg states (orbital angular momentum $\ell \leq 2$ in rubidium) produce molecules with $\sim$ MHz binding energies and permanent electric dipole moments of a few Debye. The $\ell = 0$ molecules were first observed by photoassociation [10] of cold ^{87}Rb atoms [2]. Recently, molecular states with $\ell = 1$ and high electron energies have also been excited via bound-bound transitions in $^{85}\mathrm{Rb}_2$ [9]. For high-ℓ Rydberg states, so-called trilobite molecules with giant permanent electric dipole moments of several kilo-Debye and $\sim$ GHz binding energies are predicted to exist [1]. These have yet to be observed, though dipolar molecules have been prepared in Rb [7] and Cs [8].

The relevant interaction was first described by Fermi [11] to help explain pressure-induced energy shifts of Rydberg absorption lines in a gas [12]. The de Broglie wavelength of the Rydberg electron (position $\mathbf{r}$) is much larger than that of a heavy ground-state atom (position $\mathbf{R}$) that lies within the Rydberg atom's volume, and their interaction can be approximated as a low-energy s-wave scattering process (scattering length a_s). The interaction is described with a Fermi-type pseudopotential [1,13] $V_{\mathrm{pseudo}}(\mathbf{r}) = 2\pi a_s \delta^3(\mathbf{r} - \mathbf{R})$, where p-wave and higher-order scattering [4] are neglected. For negative a_s, the interaction can lead to bound molecular states [1,13].

The bond strengths and electric and magnetic moments of Rydberg molecules are strongly dependent on the angular-momentum couplings in the Rydberg and ground-state atom constituents. In the present work, we focus on long-range $^{87}\mathrm{Rb}_2$ molecules formed by an nD Rydberg and a $5S_{1/2}$ ground-state atom. Within the low-ℓ class of these molecules, the nD ones have the highest binding energies, which generally increase with ℓ due to the $\sqrt{2\ell + 1}$ scaling of the angular wave functions $Y_l^{m=0}(\theta = 0)$. The angular-momentum coupling spans three Hund's cases as ℓ varies from 0 to 2. The $nS_{1/2} + 5S_{1/2}$ molecules are akin to Hund's case (b), because they have $L = 0$ and total electron spin $S = 1$. The $nP_j + 5S_{1/2}$ molecules are akin to Hund's case (c), because the fine structure coupling is larger than the scattering interaction energy. The $nD_j + 5S_{1/2}$ molecules present a unique system, because they transition from Hund's case (c) at large n to Hund's case (a) at $n \lesssim 30$, where the scattering interaction energy becomes increasingly greater than the fine structure coupling. The F and higher-ℓ states of Rb intersect with a sole, deeply bound (trilobite) potential which accumulates most of the level shifts [1], negating the existence of potential wells similar to those below the S, P, and D asymptotes. In our model, we include the fine structure of the Rydberg atom and the hyperfine structure of the $5S_{1/2}$ perturber atom, both of which have observable effects.

To excite nD Rydberg molecules, we first prepare a sample of $\sim 10^5$ magnetically trapped ^{87}Rb atoms in their $|F = 2, m_F = 2\rangle$ ground state at a temperature ≤ 17 μK and peak density $\gtrsim 5 \times 10^{11}$ cm^{-3}. Optical excitation to nD Rydberg states is accomplished via a two-photon transition from the $5S_{1/2}$ ground state by using 780- and 480-nm laser beams. The 780-nm laser frequency is fixed $\sim$1 GHz off resonance from the $5S_{1/2}$ to $5P_{3/2}$ transition, and the 480-nm laser frequency is scanned to excite either Rydberg atoms or

molecules. The combined excitation bandwidth is ≈2 MHz. The 780-nm laser has a power of ∼500 μW and is collimated to a full width at half maximum (FWHM) of 3.5 mm. The 480-nm beam has a power of ∼35 mW and is focused to a FWHM of 89 ± 5 μm into the cigar-shaped atom sample, which has a FWHM diameter of 28 μm and an aspect ratio of ≈1:3.

The atom sample is enclosed by six individually addressable electrodes used to control the electric field at the excitation location, described in previous work [14]. We zero the electric field to within ≲200 mV/cm by Stark spectroscopy on 59D Rydberg states [15]. This ensures that quadratic Stark shifts of the nD Rydberg levels in the n range of interest are ≲2 MHz. In a single experiment, the atom sample is illuminated by $2-3$ μs long laser pulses followed by electric-field ionization of Rydberg atoms and molecules [16]. The signal ions are extracted and detected by a microchannel plate located 10 cm away. We use one ground-state atom sample for a series of 55 individual experiments at a single 480-nm frequency step; density loss during one series is negligible.

The photoassociation of a Rydberg atom and ground-state atom pair into a bound molecular state occurs when the excitation laser is detuned from the atomic Rydberg line by an amount equal to the molecular binding energy. In Fig. 1, we show an experimental spectrum in the vicinity of the atomic $35D_{5/2}$ Rydberg line. A prominent satellite line emerges at -38 ± 3 MHz, which is assigned to the $(35D_{5/2} + 5S_{1/2})(\nu = 0)$ molecule, where $\nu = 0$ denotes the vibrational ground state. This binding energy is ≈1.6 times larger than that of the $(35S_{1/2} + 5S_{1/2})(\nu = 0)$ molecular state measured in previous experiments [2,6].

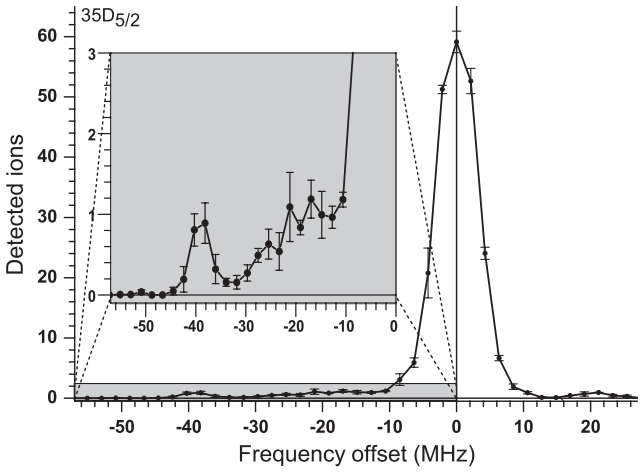

FIG. 1. Spectrum centered on the $35D_{5/2}$ atomic Rydberg line showing the ^{87}Rb$(35D_{5/2} + 5S_{1/2})(\nu = 0)$ molecular line at -38 ± 3 MHz. The vertical error bars are the standard error of three sets of 55 individual experiments at each frequency step. The error in the binding energy is equal to the average long-term frequency drift observed over one full scan.

The larger binding energy reflects the deepening of the molecular potential with ℓ.

A series of $nD_{5/2}$ Rydberg spectra for $34 \le n \le 42$ is shown in Fig. 2(a) (right). The lowermost, redshifted lines for $n = 40$ and below are assigned to the molecular states. Molecular lines are not discernable in the $n = 42$ and 41 spectra, because the line broadening due to residual fields and the laser linewidth exceeds the molecular binding energies for these states. Additional satellite lines are expected but are likely obscured in Figs. 1 and 2(a) by the broadening of the atomic lines as well as artificial signals at ±20 MHz due to weak, symmetric side peaks in the 480-nm laser spectrum (caused by a Pound-Drever-Hall stabilization loop). Features near −20 MHz are assigned to molecular lines only if they are significantly stronger than the artificial signal at +20 MHz.

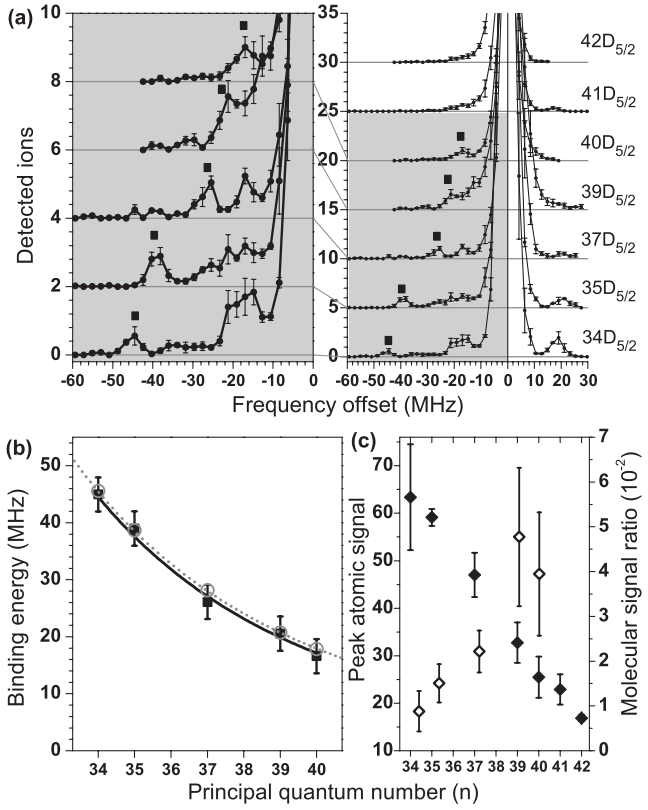

FIG. 2. (a) Right: Spectra centered on $nD_{5/2}$ atomic Rydberg lines for the indicated values of n and identified molecular lines (squares). Left: Selected spectra from the plot on the right for states with identified molecular lines. Error bars are obtained as in Fig. 1. (b) Binding energies obtained from Gaussian fits to the molecular lines identified in (a) vs n. An allometric fit (solid curve) to the experimental binding energies yields a $n^{-5.9\pm0.4}$ scaling. Also shown are theoretical binding energies for the ^{87}Rb$(nD_{5/2} + 5S_{1/2})(\nu = 0)$ molecular states with $a_{s0} = -14a_0$ (hollow circles and dotted curve). (c) Peak number of detected ions on the $nD_{5/2}$ atomic Rydberg line (solid diamonds, left axis) and ratio of molecular and atomic line strengths (hollow diamonds, right axis) vs n.

Figure 2(b) shows the molecular binding energies measured in Fig. 2(a) vs n. One may expect the binding energies to be proportional to the probability density of the Rydberg electron wave function, which scales as $\sim n^{-6}$. An allometric fit to the data in Fig. 2(b) qualitatively supports this expectation over the displayed range of n.

As shown in Fig. 2(c), the ratio of molecular and atomic line strengths ranges from $\approx 1\% - 5\%$. By taking our peak atomic density into consideration, this agrees quite well with the relative signal strengths found in Refs. [2,6]. One may expect the molecular-signal ratio to scale with the probability of finding a $5S_{1/2}$ atom within the Rydberg-atom volume (which scales as n^6), corresponding to an increase of about a factor of 2.5 over the n range in Fig. 2(c). The observed increase is about a factor of 5. This enhancement is likely due to a Rydberg excitation blockade caused by electrostatic Rydberg-atom interactions [17,18], which suppresses the atomic line [19]. Since the blockade's effectiveness increases with n, the molecular-signal ratio scales faster than n^6. This interpretation is corroborated by the atomic-signal strength, which drops by a factor of 4 over the n range in Fig. 2(c). In the absence of an excitation blockade, the atomic signal would drop as n^{-3}, i.e., by only a factor of 2 in Fig. 2(c).

Molecular states of the $nD_j + 5S_{1/2}$ type exhibit a transition between Hund's case (a) at low n and Hund's case (c) at high n. Most of our data trend towards Hund's case (c), where the dominant molecular potentials carry spin-dependent factors $|\langle m_\ell = 0, m_s = \pm 1/2 | j, m_j = \pm 1/2\rangle|^2$ (detailed model below); these factors are $\ell/(2\ell+1)$ for $j = \ell - 1/2$ and $(\ell+1)/(2\ell+1)$ for $j = \ell + 1/2$. Hence, in Hund's case (c) (high n) the $\nu = 0$ binding-energy ratio for $nD_j + 5S_{1/2}$ $j = 3/2$ and $5/2$ molecules should be about $2/3$. For decreasing n, the fine structure splitting increases as n^{-3}, while the molecular binding energy increases as n^{-6}. The system then trends towards Hund's case (a), in which the $\nu = 0$ binding energy ratio changes from $2/3$ to $\gg 1$ (see below). Therefore, the $\nu = 0$ binding energy ratio is a convenient experimental measure to characterize the system. Figure 3 shows spectra of the two fine structure components of $37D$. Molecular peaks are present for both $j = 3/2$ and $5/2$, with binding energies of 24 ± 3 and 26 ± 3 MHz, respectively, corresponding to a ratio of 0.92 ± 0.15. Since this is significantly larger than $2/3$, for $n = 37$ the system is in the transition regime between Hund's cases (c) and (a).

Next we compare experimental data with a calculation. We consider s-wave triplet scattering and omit singlet scattering [1]. For low electron momenta k, the s-wave triplet scattering length is $a_s^T(k) \approx a_{s0} + \frac{\pi}{3}\alpha k$, where $a_{s0} = a_s^T(k=0)$ is the zero-energy scattering length and α the Rb $5S_{1/2}$ polarizability [13]. We fit a_{s0} to match the experimental data. In calculations not presented here we have verified that p-wave scattering strongly influences the inner part of the molecular potentials [20] but leaves the outermost well, where the bound states relevant to our work are found, largely unaffected. The Rydberg atom's fine structure and the perturber's hyperfine structure are included, because they are on the same order or larger than the molecular binding. The much smaller hyperfine structure of the Rydberg atom is ignored. We include configuration mixing with neighboring Rydberg manifolds [5]. For the $5S_{1/2}$ atom located at $\mathbf{R} = Z\mathbf{e}_z$, the Hamiltonian is

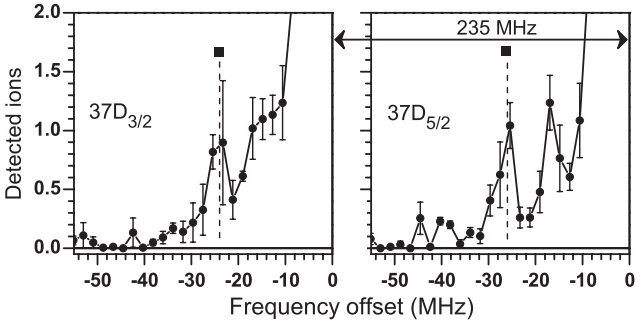

FIG. 3. Spectra centered on the $37D_j$ atomic Rydberg lines for $j = 3/2$ (left) and $j = 5/2$ (right; the same as in Fig. 2). $^{87}\mathrm{Rb}(37D_j + 5S_{1/2})(\nu = 0)$ molecular signals are indicated by vertical dashed lines and squares.

$$\hat{H}_0 + 2\pi a_s^T[k(r)]\delta^3(\hat{\mathbf{r}} - Z\mathbf{e}_z)\left(\hat{\mathbf{S}}_1 \cdot \hat{\mathbf{S}}_2 + \frac{3}{4}\right) + A\hat{\mathbf{S}}_2 \cdot \hat{\mathbf{I}}_2, \tag{1}$$

where the unperturbed Hamiltonian $\hat{H}_0$ includes Rydberg quantum defects and fine structure [16]. The operators $\hat{\mathbf{S}}_1$ and $\hat{\mathbf{S}}_2$ are the spins of the Rydberg electron and $5S_{1/2}$ atom, respectively. The ^{87}Rb $5S_{1/2}$ atom has $\ell_2 = 0$, a nuclear spin $\hat{\mathbf{I}}_2$ with $I_2 = 3/2$, and a hyperfine parameter $A = h \times 3.4$ GHz (in SI units). The projector $\hat{\mathbf{S}}_1 \cdot \hat{\mathbf{S}}_2 + \frac{3}{4}$ has the eigenvalue one (zero) for the triplet (singlet) states of $\hat{\mathbf{S}}_1$ and $\hat{\mathbf{S}}_2$, enabling only triplet scattering. In the classically allowed range of the Rydberg electron $k = \sqrt{-1/(n_{\mathrm{eff},1}n_{\mathrm{eff},2}) + 2/r}$ (atomic units), and $k = 0$ elsewhere. There, $n_{\mathrm{eff},1}$ and $n_{\mathrm{eff},2}$ are the effective quantum numbers of the Rydberg states coupled by the scattering term. Since only states with $m_{\ell 1} = 0$ are nonvanishing on the internuclear axis, the relevant Hilbert space is limited to $\{|n, \ell_1, j_1, m_{j1} = \pm 1/2, m_{s2} = \pm 1/2, m_{i2} = \pm 1/2, \pm 3/2\rangle\}$. Since the Hamiltonian in Eq. (1) conserves $m_k := m_{j1} + m_{s2} + m_{i2}$, the space breaks up into separated subspaces with $m_k = \pm 5/2$, $\pm 3/2$, $\pm 1/2$, where the scattering term couples states with the same $m_{j1} + m_{s2}$, while the hyperfine term couples states with the same $m_{s2} + m_{i2}$.

The Hamiltonian in Eq. (1) is diagonalized, resulting in adiabatic potential surfaces $V_{ad,i}(Z)$ and electric $[d_i(Z)]$ and magnetic $[\mu_i(Z)]$ dipole moments of the adiabatic

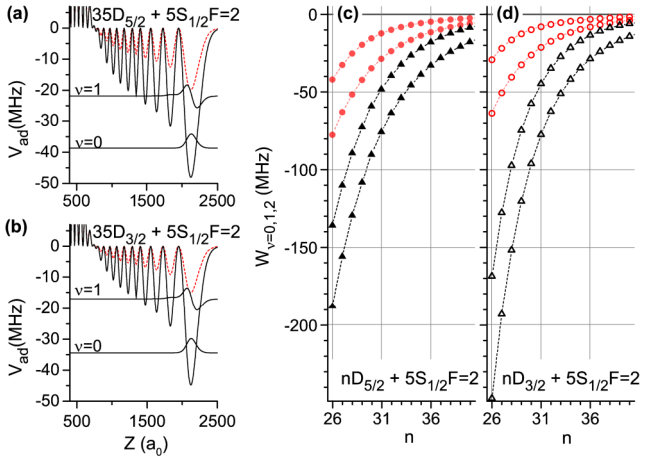

FIG. 4 (color online). (a),(b) Deep (solid lines) and shallow (dashed lines) potentials for $35D_{3/2}$ and $35D_{5/2}$-type molecules, for $a_{s0} = -14a_0$, and vibrational wave functions for $\nu = 0$, 1 in the deep potentials. (c),(d) Energy levels for $\nu = 0$, 1 in the deep (triangles) and shallow (circles) potentials vs n.

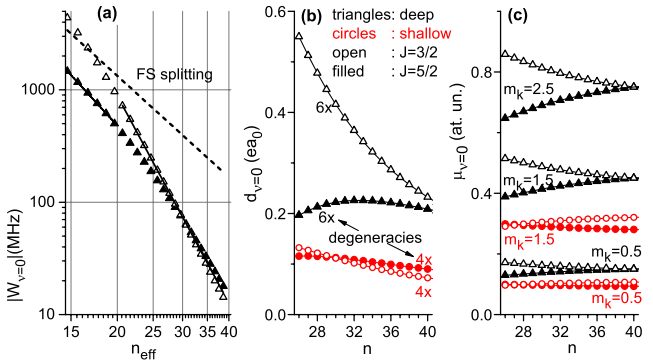

FIG. 5 (color online). (a) $\nu = 0$ binding energies in the deep molecular potentials for $nD_{5/2}$ (filled triangles), $nD_{3/2}$ (open triangles), and the D fine structure splitting (dashed line) vs the effective quantum number. Solid lines are fits. The $D_{3/2}$ energies are fit well by 84.2 GHz$/n_{\rm eff}^{6.13}$. The $D_{5/2}$ energies do not exhibit a global scaling; at low n they tend to scale as 23 MHz$/n_{\rm eff}^{3.6}$. (b) Electric dipole moments for $\nu = 0$ vs n for the deep (triangles) and shallow (circles) $V_{\rm ad}(Z)$ for $j = 3/2$ (open) and $j = 5/2$ (filled). (c) Magnetic dipole moments for the same states as in (b).

states [i is an arbitrary label for the $V_{ad}(Z)$]. The vibrational states $W_{i,\nu}$ and their wave functions $\Psi_{i,\nu}(Z)$ are found by solving the Schrödinger equation with potential $V_{ad,i}(Z)$ and reduced mass 87 amu/2, and their electric and magnetic dipole moments are $d_{i,\nu} = \int |\Psi_{i,\nu}(Z)|^2 d_i(Z) dZ$ and $\mu_{i,\nu} = \int |\Psi_{i,\nu}(Z)|^2 \mu_i(Z) dZ$, respectively.

In Figs. 4(a) and 4(b), we show all potentials $V_{ad}(Z)$ for $35D_{5/2}$ and $35D_{3/2}$ that connect to the $F = 2$ hyperfine level of the $5S_{1/2}$ atom, as well as the vibrational states $\nu = 0$, 1 of the deeper potentials. The deep and shallow potentials and their states have degeneracies of 6 and 4, respectively. The shallow potentials are due to hyperfine-induced mixing between the electronic singlet and a triplet state. In Figs. 4(c) and 4(d), we show the vibrational energies $W_{i,\nu}$ for $\nu = 0$, 1 over a range of n for $nD_{5/2} + 5S_{1/2}$ and $nD_{3/2} + 5S_{1/2}$ molecules.

In the experiment, we excite molecules below the $F = 2$ asymptote, for which the states in the deep potential $V_{ad}(Z)$ have the larger degeneracy and are easier to observe due to their larger binding energies. Hence, we adjust a_{s0} so that the $\nu = 0$ levels in the deep $V_{ad}(Z)$ match the experimental data in Figs. 1–3 and find $a_{s0} = -14a_0 \pm 0.5a_0$ [see Fig. 2(b)]. (For $37D_{5/2}$ the $\nu = 0$ binding energy increases by about 4 MHz when changing a_{s0} from -13.5 to $-14.5a_0$.) This a_{s0} value lies within the range of published values -13 to $-19.48a_0$ [2,6,21–23]. The experimental signals at about half the $\nu = 0$ binding energies, seen in some of the plots in Fig. 2(a), may correspond to levels at about half the $\nu = 0$ binding energies in Figs. 4(c) and 4(d).

In the high-n limit in Fig. 5(a), the $\nu = 0$ binding-energy ratio for $D_{3/2}$ and $D_{5/2}$ approaches 2/3, as expected for Hund's case (c), and both sets of binding energies approximately scale inversely with the atomic volume (i.e., as $n_{\rm eff}^{-6}$). At low n, the system transitions into Hund's case (a), where the binding-energy ratio changes from 2/3 to $\gg 1$. Also, the $\nu = 0$ binding energies for the lower ($D_{3/2}$) fine structure level exceed the fine structure coupling and keep scaling as $n_{\rm eff}^{-6}$, while those for the $D_{5/2}$ level approach the fine structure splitting and its scaling ($n_{\rm eff}^{-3}$). The experimental data in Fig. 3 are in the transition regime between the two Hund's cases.

For nD Rydberg molecules the electric dipole moments $d_{\nu=0}$ are somewhat smaller than for nS ones [see Fig. 5(b) and Ref. [7]]. As a result of the transition between two Hund's cases, the $d_{\nu=0}$ of the $nD_{5/2}$-type molecules do not exhibit a clear scaling. Those for the $nD_{3/2}$-type molecules scale close to $n_{\rm eff}^{-2}$, similar to S-type ones [7]. Noting that $d_{\nu=0} \lesssim 0.25ea_0$ and that the stray electric field in our experiment is $\lesssim$200 mV/cm, the experimental permanent-electric-dipole shift is well below 1 MHz. The magnetic moments [Fig. 5(c)] exhibit a gradual change that reflects the change in angular-momentum coupling behavior between the two Hund's cases. In our < 1 G magnetic field in the atom trap, the molecular lines could be broadened over a range $\lesssim$4 MHz, while the atomic lines have $|m_j| \leq 5/2$ and could be broadened over a range $\lesssim$8 MHz. These estimates agree well with the linewidths seen in the spectra.

In summary, we have observed polar Rydberg molecules of the type $nD_j + 5S_{1/2}$. The binding energies are larger than those of previously observed $nS_{1/2} + 5S_{1/2}$ molecules. The molecules undergo a transition between Hund's case (a) at low n to Hund's case (c) at high n. With improved spectroscopic resolution, one should be able to measure the electric dipole moments and to assign higher-lying vibrational levels in the deep potentials in Fig. 4 as well as levels in the shallow potentials. Recently, we became

aware of related work on nD molecular states in a higher-magnetic-field regime [24].

This work was supported by the AFOSR (FA9550-10-1-0453). We thank C. H. Greene, H. R. Sadeghpour, and S. T. Rittenhouse for helpful discussions.

*anderda@umich.edu

[1] C. H. Greene, A. S. Dickinson, and H. R. Sadeghpour, Phys. Rev. Lett. **85**, 2458 (2000).
[2] V. Bendkowsky, B. Butscher, J. Nipper, J. P. Shaffer, R. Löw, and T. Pfau, Nature (London) **458**, 1005 (2009).
[3] S. D. Hogan and F. Merkt, ChemPhysChem **10**, 2931 (2009).
[4] A. A. Khuskivadze, M. I. Chibisov, and I. I. Fabrikant, Phys. Rev. A **66**, 042709 (2002).
[5] H. R. Sadeghpour and S. T. Rittenhouse, Mol. Phys. **111**, 1902 (2013).
[6] V. Bendkowsky, B. Butscher, J. Nipper, J. B. Balewski, J. P. Shaffer, R. Löw, T. Pfau, W. Li, J. Stanojevic, T. Pohl, and J. M. Rost, Phys. Rev. Lett. **105**, 163201 (2010).
[7] W. Li, T. Pohl, J. M. Rost, S. T. Rittenhouse, H. R. Sadeghpour, J. Nipper, B. Butscher, J. B. Balewski, V. Bendkowsky, R. Löw, and T. Pfau, Science **334**, 1110 (2011).
[8] J. Tallant, S. T. Rittenhouse, D. Booth, H. R. Sadeghpour, and J. P. Shaffer, Phys. Rev. Lett. **109**, 173202 (2012).
[9] M. A. Bellos, R. Carollo, J. Banerjee, E. E. Eyler, P. L. Gould, and W. C. Stwalley, Phys. Rev. Lett. **111**, 053001 (2013).
[10] K. M. Jones, E. Tiesinga, P. D. Lett, and P. S. Julienne, Rev. Mod. Phys. **78**, 483 (2006).
[11] E. Fermi, Nuovo Cimento **11**, 157 (1934).
[12] E. Amaldi and E. Segr, Nuovo Cimento **11**, 145 (1934).
[13] A. Omont, J. Phys. (Paris) **38**, 1343 (1977).
[14] D. A. Anderson, A. Schwarzkopf, R. E. Sapiro, and G. Raithel, Phys. Rev. A **88**, 031401 (2013).
[15] J. Neukammer, H. Rinneberg, K. Vietzke, A. König, H. Hieronymus, M. Kohl, H. J. Grabka, and G. Wunner, Phys. Rev. Lett. **59**, 2947 (1987).
[16] T. F. Gallagher, *Rydberg Atoms* (Cambridge University Press, Cambridge, England, 1994), pp. 220–221.
[17] A. Reinhard, T. C. Liebisch, B. Knuffman, and G. Raithel, Phys. Rev. A **75**, 032712 (2007).
[18] A. Schwarzkopf, R. E. Sapiro, and G. Raithel, Phys. Rev. Lett. **107**, 103001 (2011).
[19] D. Tong, S. M. Farooqi, J. Stanojevic, S. Krishnan, Y. P. Zhang, R. Côté, E. E. Eyler, and P. L. Gould, Phys. Rev. Lett. **93**, 063001 (2004).
[20] E. L. Hamilton, C. H. Greene, and H. R. Sadeghpour, J. Phys. B **35**, L199 (2002).
[21] C. Bahrim and U. Thumm, Phys. Rev. A **61**, 022722 (2000).
[22] C. Bahrim, U. Thumm, and I. I. Fabrikant, J. Phys. B **34**, L195 (2001).
[23] I. I. Fabrikant, J. Phys. B **19**, 1527 (1986).
[24] A. T. Krupp, A. Gaj, J. B. Balewski, P. Ilzhöfer, S. Hofferberth, R. Löw, T. Pfau, M. Kurz, and P. Schmelcher, Phys. Rev. Lett. **112**, 143008 (2014).